Carbon Materials with Nano-sized Pores Derived from Carbides

Shinji ISHIKAWA*, Takahiro SAITO and Kazuya KUWAHARA

Materials that have a nanoscale pore structure show specific characteristics in absorbing raw materials or ions. This paper presents evaluation results of nano structure carbon materials that were obtained by treating carbide in a chlorine atmosphere. We generated the nano porous structure by processing SiC, TiC, and Al_4C_3 in a chlorine controlled atmosphere at over 1,000°C. With carbon derived from TiC and Al_4C_3, graphite structures were formed, and sub-nano pores and crystal growth reduced with increasing treatment temperature. In contrast, SiC-derived carbon did not form a graphite layer structure and maintained sub-nano pores even at high temperature of 1,400°C. With this process, we can form porous carbon materials with various characteristics by using different raw materials and temperatures. These materials can be used for a wide range of applications such as gas absorption and electricity storage.

Keywords: porous, carbon, carbide, micro-pore

1. Introduction

Nano-porous structure materials include activated-carbon, silica or alumina gel, and zeolite, which have been known since ancient times. These materials are used to absorb various substances and to provide a field that facilitates chemical reaction, as with catalyst carriers. The recent evolution of nanotechnology has led to studies of nanostructures with a more precisely controlled pore size. Strenuous efforts are being made to develop these materials to meet requirements associated with energy storage and energy conservation in chemical reactions with the objective of building a low-carbon society.[1],[2] Porous bodies have established names according to pore size, as shown in Table 1. This paper uses these designations.

Table 1. Size-based classification of pores

Pore name	Pore Size
Macro Pore	< 50 nm
Meso Pore	2-50 nm
Micro Pore	2 nm < r

Carbon materials can form various nanostructures due to the variety of carbon-carbon bonds. Amorphous nanostructures, including activated carbon and carbon black, have found use in various applications, such as polymer modifiers, absorbents, and storage battery electrodes.[3]

Recent developments include the use of low-dimensional nanostructure carbon materials, such as carbon nanotubes (CNTs) and graphene, for retention of hydrogen and other gases and as an electronic material making use of their conductivity and a storage battery material utilizing their ion absorptivity. Further development efforts, however, must be made before they are commercialized because they have crystal structures and their growth rates are not sufficiently high.

Carbon nanostructures produced by decomposing silicon carbide or other inorganic carbides include graphene and CNTs, which are obtained through thermal decomposition. Porous carbon materials are also formed by chemical reaction treatment in a chlorine atmosphere, as in the case of heat-treating carbides expressed by the chemical formula MxC in Eq. (1). This process removes non-carbon component M through reaction with chlorine, re-arranges the residual carbon component, and forms pores, as shown in Fig. 1.

$$M_xC+\frac{XY}{2}Cl_2\rightarrow C+xMCl_y \quad \cdots\cdots (1)$$

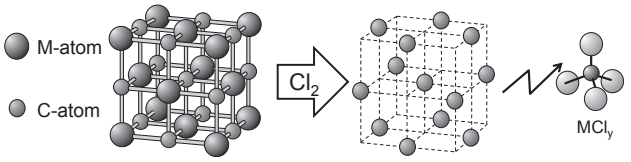

Fig. 1. Carbide-derived carbon formation process

Reports on this process exist.[4],[5] This process has proven itself to form a carbon material with an extremely large specific surface area, which is termed carbide-derived carbon (CDC). In recent years, vigorous studies have been conducted on this process to use it for the production of gas absorbents, electrode materials for electric double layer capacitors, and nano-diamonds.[6]-[9]

The present report on carbide-derived carbon, i.e. porous carbon materials made from an inorganic crystal, provides the evaluation results of the effects of chlorination temperatures on the pore structures of three types of carbide: silicon carbide (SiC), titanium carbide (TiC), and aluminum carbide (Al_4C_3).

2. Experimental

2-1 Raw materials and chlorination method

Commercially available high-purity reagent grades of SiC, TiC, and Al_4C_3 were the carbides used as raw materials (hereinafter, resultant materials are referred to as SiC-CDC, TiC-CDC, and AlC-CDC). For reaction rate evaluation, polycrystalline SiC plates of at least 99% density were used.

Each powder reagent placed in a graphite container was subjected to treatment by electrical resistance heating in a chlorine gas atmosphere to prepare porous carbon. Chlorine and nitrogen gases were mixed at a ratio of 1:10. The heating temperature range was between 1000°C and 1500°C.

2-2 Analysis method

The crystal structures of the samples were analyzed by powder X-ray diffraction (XRD) using the Cu-kα ray. The resultant diffraction patterns were used for evaluation. More specifically, the crystallite size was evaluated from the full width at half maximum of the diffraction pattern of the graphite (002) crystal plane. The interlayer spacing was evaluated according to the peak angle determined after removal of small-angle scattering from the pattern.

Pore properties were evaluated as follows. The specific surface area was calculated by the BET method*2 based on the N_2 gas adsorption isotherm*1 obtained at the temperature of liquid nitrogen. The t-plot method*3 was used to derive the volume of micropores 2 nm or less in pore diameter. The BJH analysis method*4 was used to derive the volume of mesopores 2 to 50 nm in pore diameter.

For microscopic structural evaluations, the nanostructures of samples sliced by a focused ion beam or crushing system were observed with a transmission electron microscope (TEM), and the microstructures of powders were evaluated with a scanning electron microscope (SEM).

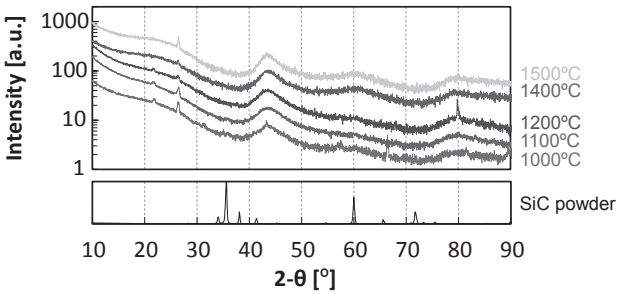

Fig. 2. XRD patterns for SiC-CDC varying with treatment temperature

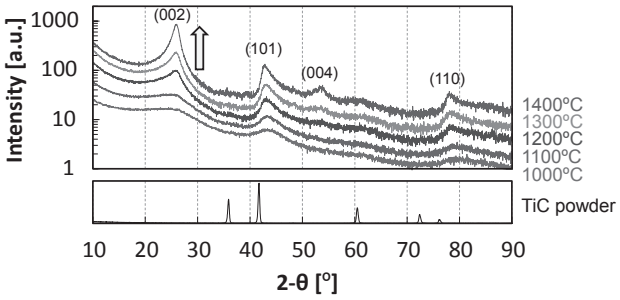

Fig. 3. XRD patterns for TiC-CDC varying with treatment temperature

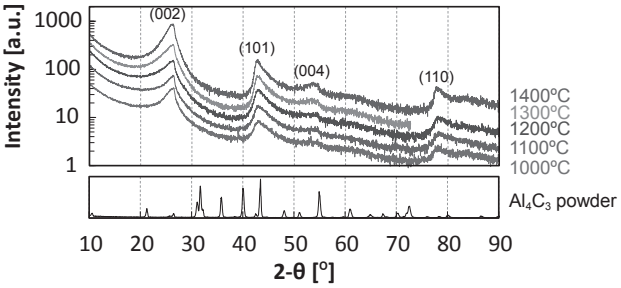

Fig. 4. XRD patterns for AlC-CDC varying with treatment temperature

3. Properties of Carbide-Derived Carbon

3-1 Crystal structure

Figures 2 to 4 show XRD patterns for SiC-CDC, TiC-CDC, and AlC-CDC along with the patterns for the raw materials. Every carbide sample lost its initial crystal structure and exhibited the diffraction peak of the graphite (002) plane in the range of $2\theta \approx 20°$ to 30°, which is specific to amorphous carbon, and the diffraction peak of the (01) plane in the range of 42° to 43°.[10] The materials TiC-CDC and AlC-CDC had a structure resembling the interlayer spacing of graphite, with the peak of the graphite (002) plane located close to 26°, while SiC-CDC exhibited a peak at a point close to 20°, demonstrating resultant substantial differences in graphite layer structure that depend on the starting materials.

The material SiC-CDC exhibited no substantial change in crystal structure even at high chlorination temperatures. In contrast, TiC-CDC presented more crystal growth at higher chlorination temperatures, as indicated by sharper crystal peaks with increasing chlorination temperatures. For AlC-CDC, changes in peak width were small even at high temperatures, with a (002) plane feature being formed by chlorination at as low as 1000°C. Moreover, AlC-CDC presented a characteristic asymmetric peak form.[11],[12]

Figure 5 shows temperature dependence of crystallite size. The results for TiC-CDC were increasing crystallite size with increasing chlorination temperatures, growing to 7 nm at 1400°C. In contrast, AlC-CDC exhibited almost no temperature-dependent change in crystallite size, reaching 2 nm in the range from 1000°C to 1400°C.

Figure 6 shows temperature dependence of interlayer spacing. The interlayer spacing of TiC-CDC approached toward that of graphite, or 0.335 nm, with the growth of crystallite, while with AlC-CDC, the effects of temperature were small, as for the crystallite size.

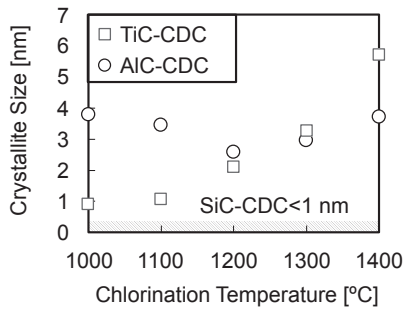

Fig. 5. Temperature dependence of crystallite size

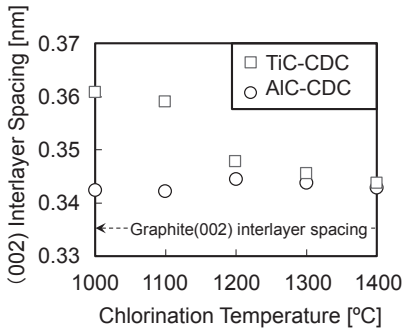

Fig. 6. Temperature dependence of interlayer spacing of graphite (002)

3-2 Pore structure

Figure 7 shows adsorption isotherms of SiC-CDC in a chlorination temperature range of 1000°C to 1500°C. The adsorption isotherms remained in Type I even at 1500°C. This result, in conjunction with the XRD analysis results, proves that the sub-nano pore structure of SiC-CDC is thermally stable.

Figure 8 shows N_2 adsorption isotherms of TiC-CDC at 77 K. After chlorination between 1000°C and 1100°C, the forms of the adsorption isotherms were typical Type I, with which the amount of adsorbate almost saturates in the low pressure range of (P/P0) < 0.1, revealing the dominant presence of micropores. At high chlorination temperatures, the adsorption volume for P/P0 < 0.1 substantially decreased, with a slope occurring in the P/P0 = 0.2 to 0.9 region. This change is interpreted as being due to micropores being lost simultaneously with the development of mesopores, with the adsorption isotherms turning to a composite type of Type I and Type IV, and, at the highest chlorination temperature of 1400°C, turning to Type II with no micropores observed or with macropores constituting the dominant structure. Phenomenologically, it is quite probable that sintering or crystal growth achieved by heat treatment caused micropores to collapse and become integrated into mesopores. One exceptional point with TiC-CDC is that a comparison of 1000°C and 1100°C isotherms reveals an increase in total pore volume resulting from chlorination at 1100°C. In light of almost the same weight loss rate, the carbon skeleton presumably expanded along with the collapse of the crystal structure.

The material AlC-CDC exhibited composite adsorption isotherms of Types I, II, and IV through chlorination at as low as 1000°C as in Fig. 9. Its micropores decreased with increasing chlorination temperatures, as in the case of TiC-CDC.

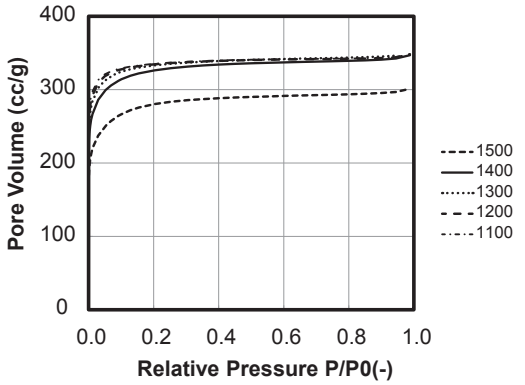

Fig. 7. Adsorption isotherms for SiC-CDC varying with temperature

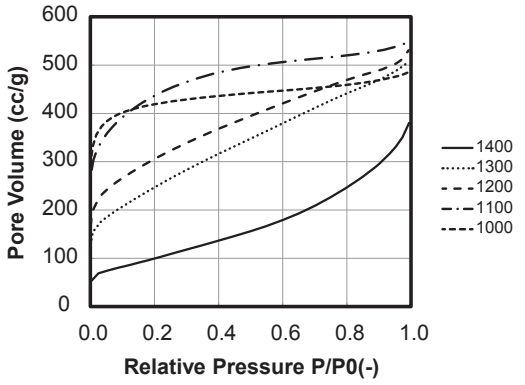

Fig. 8. Adsorption isotherms for TiC-CDC varying with temperature

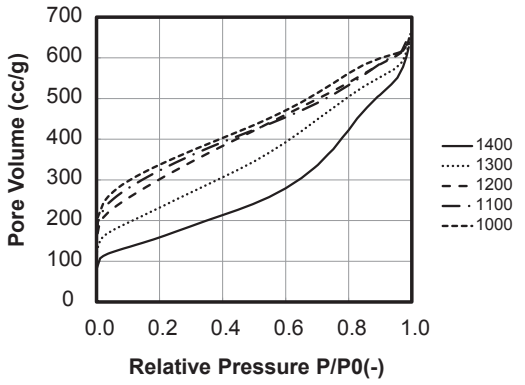

Fig. 9. Adsorption isotherms for AlC-CDC varying with temperature

Figures 10, 11 and 12 show relationships between chlorination temperature and specific surface area and between chlorination temperature and pore structure. With TiC-CDC and AlC-CDC, the BET specific surface area and the volume of micropores decreased with increasing chlorination temperatures while the volume of mesopores increased. On the other hand, SiC-CDC exhibited almost no temperature dependence of either BET specific surface area or volume of mesopores between 1000°C and 1500°C.

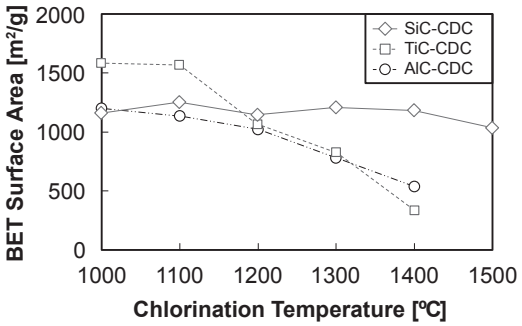

Fig. 10. Temperature dependence of BET specific surface area

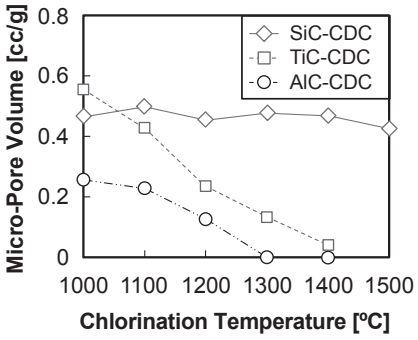

Fig. 11. Temperature dependence of volume of micropores (< 2 nm)

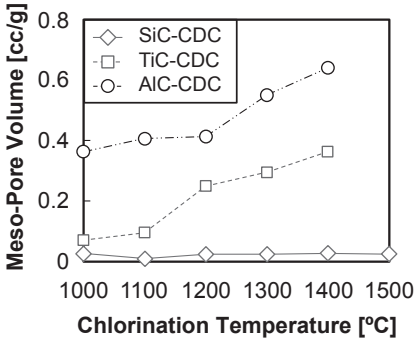

Fig. 12. Temperature dependence of volume of mesopores (< 2 to 50 nm)

3-3 Discussion about carbon structures

As discussed above, porous CDC materials of various pore structures are produced from different starting materials. Figure 13 schematically shows the structural changes that take place when carbide is converted into carbon. It is quite probable that in the case of TiC-CDC, two-dimensional arrays that serve as the base of the graphite layer structure are formed during conversion into carbon. As the graphite structure grows with increasing treatment temperatures, solid portions shrink, resulting in the formation of a meso-pore structure. In contrast, with SiC-CDC, carbon faces presumably form three-dimensionally folded arrays during conversion into carbon, inhibiting thermal re-arranging and retaining random arrays, although being subject to slight shrinkage.

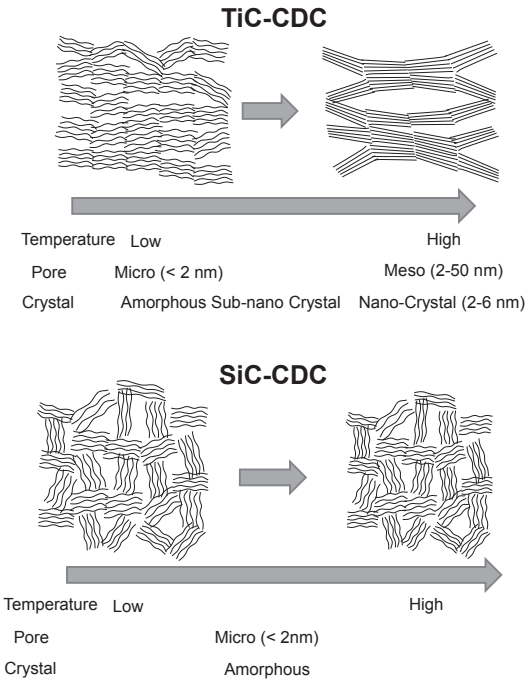

Fig. 13. Structures of TiC-CDC and SiC-CDC varying with temperature

3-4 Microscopic structures

Photo 1 shows a high-resolution TEM image of the marginal portion of a SiC-CDC powder sample. The photograph reveals an approximately 0.5 nm turbostratic carbon structure. This turbostratic structure is thought to correspond to the broad diffraction peak near 20° in XRD patterns. Moreover, the turbostratic structure forms several-nanometer domains. This nano-structure is likely to be the cause of small-angle scattering in XRD. Photo 2 shows structures observed near the reaction interface. The gray area represents carbon converted from SiC. The black area represents SiC. This photograph reveals a sharp several nanometer-thick reaction interface.

Photo 3 shows an SEM image of SiC-CDC 100 μm in mean particle size. Fracture faces of SiC particles have a shell-like structure because they are produced by crushing. This structure is retained in CDC converted from SiC. Hence they have no changes in macrostructure even after conversion into carbon. This implies that unlike conversion of resin into carbon, it is not necessary to consider changes in size resulting from conversion of SiC into carbon. In other words, the CDC formation process is advantageous in controlling the geometry of micropore structures.

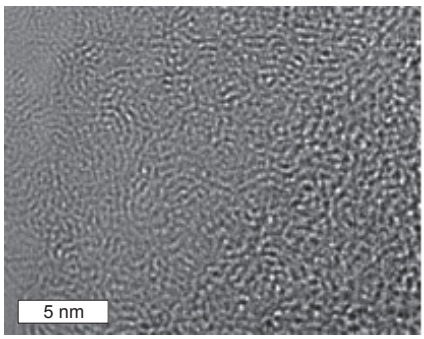

Photo 1. TEM image of microscopic structure of SiC-CDC

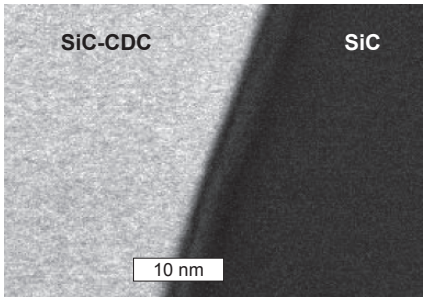

Photo 2. Microscopic structure of SiC-CDC at reaction interface

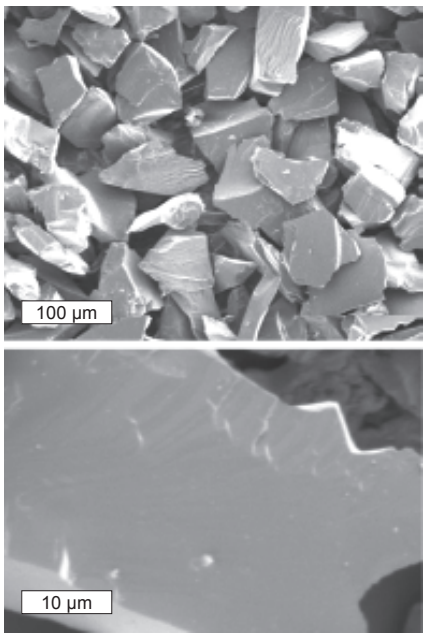

Photo 3. SEM images of particulate structure of SiC-CDC

4. Evaluation of Reaction Rates

Free energy change in reaction between carbide and chlorine gas manifests as an exothermal reaction above ordinary temperatures in the case of SiC. For industrial use of materials, it is necessary to clearly establish reaction conditions, such as temperature and reaction gas concentration. This section presents the results of evaluation of reaction rates, using thicknesses of carbon layers produced via reaction of closely packed plate samples as a measure of evaluation.

Figure 14 shows reaction rates normalized by the carbon layer production rate determined at 900°C, plotted against inverse absolute temperatures. The reaction rates exhibited temperature dependence conforming very closely to the Arrhenius equation, as illustrated in the figure. Activation energy determined by the resultant temperature dependence of reaction rates was approximately 160 kJ/mol. This value is roughly the same as the temperature dependence of etching rates observed in etching of SiC semiconductors by chlorine gas.[13]

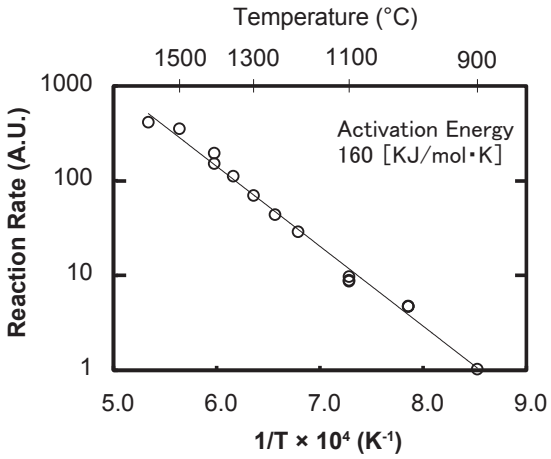

Fig. 14. Temperature dependence of SiC-CDC reaction rate

5. Conclusion

The present study evaluated prototype porous carbon materials that have a nano-pore structure, which were formed from inorganic carbides by removing carbonized components through chlorination. The study revealed that achieved carbon materials exhibit substantially varying properties depending on the starting carbide material and treatment temperature.

With SiC-CDC, the porous structure ranged from 0.5 to 0.6 nm in pore size and was stable even at a high chlorination temperature of 1400°C.

The materials TiC-CDC and AlC-CDC formed porous solid comprising nanoscale graphite crystals. The pore sizes of these materials can be tailored to micropores or to mesopores by controlling the chlorination temperature.

These types of materials can be formed in a simple reaction system that performs chlorination, at a relatively high reaction rate, and on a mass production scale. Future tasks include application of the achieved pore structures to various areas such as electricity storage, molecular filters, and adsorbents.[14] Meanwhile, it is possible to make the manufacturing process closed, by recycling the reaction components and other means.[15],[16] We intend to promote the use of these products as useful materials for building a low-carbon society and enabling efficient energy use.

Technical Terms

∗1 Adsorption isotherm: An adsorption isotherm is a graph that plots relationships between pressure and the amount of adsorbate measured at constant temperature of the object under measurement. The International Union of Pure and Applied Chemistry (IUPAC) has defined the following six types of typical isotherms.
Type I: materials that have micropores; Types II and III: non-porous materials; Types IV and V: materials that have mesopores; and Type VI: non-porous plates

∗2 BET method: A method of calculating specific surface areas, derived from a model which forms multilayers of nitrogen molecules on its surface

∗3 t-plot method: A micropore distribution calculation method, which analyzes the amount of adsorbate in terms of thickness of adsorbate molecules

∗4 BJH analysis method: An analysis method used to determine pore distributions by assuming the occurrence of capillary condensation and calculating how much the volume of pores that are free of capillary condensation accounts for in total pore volume, with calculation starting from higher relative-pressure regions

References

(1) "New Development of Inorganic Porous Materials," TORAY Research Center, Inc. (2014)
(2) K. Kaneko et al., Zeolite News Letter 29, pp10-21 (2012)
(3) M. Inagaki, "Carbon Old but New Material," Morikita Publishing Co., Ltd. (2011)
(4) W. A. Mohun, US patent No. 3066099 (1962)
(5) S. Ishikawa et al., Japan Patent Publication number H02-184511 (1990)
(6) V. Presser et al., Adv. Funct. Mater. 21, pp 810-833 (2011)
(7) J. Chmiola et al., Science 313 pp1760-1763 (2006)
(8) J. A. Fernández et al., Electrochimica Acta 53, pp7111-7116 (2008)
(9) S. Welz et al., J. Appl. Phys. 93,pp4207-4214 (2003)
(10) M. Inagaki, "Carbon Material Engineering," pp3-6, THE NIKKAN KOGYO SHIMBUN, LTD. (1985)
(11) T. Saito et al., The 75th JSAP Autumn Meeting, 19p-B1-5 (2014)
(12) S. Ishikawa et al., The 41st Carbon Society of Japan Annual Meeting, PI02 (2014)
(13) T. Hatayama et al., IEICE Technical Report SDM2012-116, pp. 7-12 (2012)
(14) T. Saito et al., The 82th Meeting Electrochemical Society of Japan 1L08 (2015)
(15) S. Ishikawa et al., International Publication number WO2013/150941 (2013)
(16) S. Ishikawa et al., International Publication number WO2013/190945 (2013)

Contributors The lead author is indicated by an asterisk (*).

S. ISHIKAWA*

- Senior Assistant General Manager, Optical Communications Laboratory

T. SAITO

- Optical Communications Laboratory

K. KUWAHARA

- Senior Assistant General Manager, New Business Marketing & Promotion Division